On the thermodynamic stability of polycations

Denis S. Tikhonov[1,*], Jason W.L. Lee[1], and Melanie Schnell[1,2,*]

[1]Deutsches Elektronen-Synchrotron DESY, Notkestr. 85, 22607 Hamburg, Germany
[2]Institute of Physical Chemistry, Christian-Albrechts-Universität zu Kiel, Max-Eyth-Str. 1, 24118 Kiel, Germany
[*]denis.tikhonov@desy.de, melanie.schnell@desy.de

May 30, 2024

We present a simple approximation to estimate the largest charge that a given molecule can hold until fragmentation into smaller charged species becomes more energetically favorable. This approximation solely relies on the ionization potentials, electron affinities of the parent and fragment species, and also on the neutral parent's dissociation energy. By parametrizing these quantities, it is possible to obtain analytical phase diagrams of polycationic stability. We demonstrate the applicability of this approach by discussing maximal charge dependence on the size of the molecular system. A numerical demonstration for linear polyenes, monocyclic annulenes, and helium clusters is provided.

1 Introduction

Molecular composition in the interstellar medium (ISM) is rich: so far, more than 300 molecular species have been identified through their spectroscopic signatures.[1] If we also include the polycyclic aromatic hydrocarbons (PAHs), which are estimated to contain up to 10% of all galactic carbon,[2] the potential molecular variety grows even larger. However, the ISM is still a harsh place for molecules: cosmic radiation from various sources provides high-energy photons that can provide single and multiple ionization of the molecular species.[1–4] For instance, if a PAH molecule will absorb an extreme UV or soft X-ray photon, this can lead up to triple ionization with a production of a stable trication and/or to fragmentation.[3, 5–7] Therefore, molecular mono- and polycations can exist in the ISM, serving as intermediates in different chemical reactions and generating new molecular species.[8] The potential role of multiply charged ions in the production of complex molecules can be crucial since the rates of ion-neutral reactions grow linearly with the increase of the ionic charge.[9]

Over the years, many experimental results were obtained in investigating molecular polycations.[10, 11] For instance, dications were detected in space, in the tails of comets,[12] trications of PAHs were produced with high-energy photons,[6] by above-threshold ionization (ATI), and also by interaction with highly-charged xenon ions.[13] The quest for molecular tetracations started with the high-power ATI by femtosecond intense laser pulses, which led to the laboratory detection of tetracations of PAHs,[14] substituted benzene,[15] and even doubly-iodosubstituted acetylene.[16] Intact tetracations of PAHs were also found in high-energy collisions of neutral PAH molecules with various ions.[17] However, to our knowledge, no existing model provides a general description of the stability of polycations. In the case of fragmentation, the availability of many possible pathways of fragmentation possibilities with various spin-charge states provides a very challenging chemical space to sample.[5, 18–22] Theoretical calculations may be done, for instance, using molecular dynamics-based approaches,[23–26] reproducing some of the polycationic properties, such as the kinetic energy release in fragmentation.[27] Semi-quantitative models are known to be useful for describing trends of different processes.[11, 28–31] In particular, a model for polycation stability based on the Coulomb interaction potential was proposed in Ref. [11], and for fullerenes, a Hückel-method [32] based model was introduced in Ref. [31].

In this work, we provide a derivation of a simple approximation to estimate the largest charge a given molecule can hold until the fragmentation of this ion into smaller charged species becomes more energetically favorable. This approximation solely relies on the ionization potentials, electron affinities of the parent and fragment species, and the neutral parent's dissociation energy. This allows for a significant reduction of the computational time for estimating the polycationic stability. The same approximation for the maximal possible charge of the molecule can be further parametrized to produce an analytical approximation for the maximum charge, depending on various molecular properties, such as the size of the molecule. We demonstrate the applicability of our approach with two showcase examples, imitating the ISM-important species. The first case is chemically-bound π-conjugated hydrocarbons: linear polyenes

and monocyclic annulenes that serve as simplified analogs of PAHs. The second case is helium clusters, illustrating the general applicability of the same approach to non-covalently bound clusters, such as PAH clusters and dust nanograins.[33]

2 Thermodynamics of the polycation's dissociation

Let us define the thermodynamic stability of the polycation through its dissociation reaction *via* the following formal chemical reaction:

$$\mathrm{P}^{Q+} \rightarrow \mathrm{X}^{q_\mathrm{X}+} + \mathrm{Y}^{q_\mathrm{Y}+} \ , \tag{1}$$

where P^{Q+}, with charge $Q \geq 0$, is either a parent neutral molecule ($Q = 0$) or a (poly)cation ($Q > 0$), and $\mathrm{X}^{q_\mathrm{X}+}$ and $\mathrm{Y}^{q_\mathrm{Y}+}$ are the daughter ions with charges $q_\mathrm{X} \geq 0$ and $q_\mathrm{Y} \geq 0$, respectively. The daughter ions' charges fulfill the charge conservation $Q = q_\mathrm{X} + q_\mathrm{Y}$. The following equation gives the dissociation energy of this reaction:

$$D_\mathrm{XY}(q_\mathrm{X}, q_\mathrm{Y}) = E_\mathrm{X}(q_\mathrm{X}) + E_\mathrm{Y}(q_\mathrm{Y}) - E_\mathrm{P}(Q) \ , \tag{2}$$

where $E_A(q)$ denotes the energy of the fragment "A" with charge q. For simplicity, we will consider only the electronic energy contribution to dissociation energy, ignoring the vibrational effects. To approximate electronic energies of molecules, we use a Taylor expansion of the following form:[34, 35]

$$E(q) \approx E(0) + \frac{dE}{dq}(0) \cdot q + \frac{1}{2}\frac{d^2E}{dq^2}(0) \cdot q^2 = E(0) + \chi q + \eta q^2 \ , \tag{3}$$

where $E(0)$ is the electronic energy of the neutral molecule, $\chi = \frac{dE}{dq}(0) = \frac{\mathrm{IP}+\mathrm{EA}}{2}$ is Mulliken's electronegativity, given through molecular ionization potential (IP) and electron affinity (EA), and $\eta = \frac{1}{2}\frac{d^2E}{dq^2}(0) = \frac{\mathrm{IP}-\mathrm{EA}}{2}$ is the Pearson's absolute hardness.[34, 35] We can apply Koopmans' theorem to calculate χ and η. This theorem states that $\mathrm{IP} = -\varepsilon_\mathrm{HOMO}$ and $\mathrm{EA} = -\varepsilon_\mathrm{LUMO}$ with ε denoting the molecular orbital's (MO) energy for the highest occupied MO (HOMO) and lowest unoccupied MO (LUMO), respectively.[36] Therefore, we can express our parameters in Equation 3 as:

$$\chi = \frac{\mathrm{IP} + \mathrm{EA}}{2} = -\frac{\varepsilon_\mathrm{LUMO} + \varepsilon_\mathrm{HOMO}}{2} \ , \tag{4}$$

and

$$\eta = \frac{\mathrm{IP} - \mathrm{EA}}{2} = \frac{\varepsilon_\mathrm{LUMO} - \varepsilon_\mathrm{HOMO}}{2} \ . \tag{5}$$

Parametrization of the electronic energy given in Equation 3 by construction provides exact values for the IP and EA of the molecule. The aforementioned approximation for the higher ionization states deviates from the actual energy values. Nevertheless, the general energy increase trend is being reproduced. For instance, for quintuply-charged benzene (C_6H_6), the approximation *via* Equation 3 overestimates the ionization energy by 36% compared to the DFT-computed value, and for [22]annulene ($C_{22}H_{22}$), the analogous overestimation is 16%. However, for lower charge states, the overestimation of the energy is smaller, which makes Equation 3 a useful parametrization of the trends for IP. A comparison of actual and estimated electronic energies for five annulenes can be found in the supporting information (SI) in Figure S1.

The expression 3 thus gives us an approximation for the polycation's dissociation energy of Equation 2:

$$\begin{aligned} D_\mathrm{XY}(q_\mathrm{X}, q_\mathrm{Y}) \approx \overbrace{E_\mathrm{X}(0) + E_\mathrm{Y}(0) - E_\mathrm{P}(0)}^{D} + \\ + \chi_\mathrm{X} q_\mathrm{X} + \eta_\mathrm{X} q_\mathrm{X}^2 + \chi_\mathrm{Y} q_\mathrm{Y} + \eta_\mathrm{Y} q_\mathrm{Y}^2 - \chi_\mathrm{P} Q - \eta_\mathrm{P} Q^2 = \\ = D + \chi_\mathrm{X} q_\mathrm{X} + \eta_\mathrm{X} q_\mathrm{X}^2 + \chi_\mathrm{Y} q_\mathrm{Y} + \eta_\mathrm{Y} q_\mathrm{Y}^2 - \chi_\mathrm{P} Q - \eta_\mathrm{P} Q^2 \ , \end{aligned} \tag{6}$$

where $D = D_\mathrm{XY}(0, 0)$ is the dissociation energy of the neutral molecule. For a polycation with charge Q to be thermodynamically stable, all possible dissociation energies for all dissociation reactions of the type 1 should be endothermic, i.e., the thermodynamic stability condition is:

$$\min\{D_\mathrm{XY}(q_\mathrm{X}, q_\mathrm{Y})\} \geq 0 \ , \tag{7}$$

which should be fulfilled for all combinations of the daughter species "X" and "Y" and their charges q_X and q_Y. For a given set of daughter fragments and the dissociation energy approximation from Equation 6, we can find the minimum

dissociation energy by varying the charges q_X and q_Y with the charge conservation conditions $Q = q_X + q_Y$. This can be easily done using the Lagrangian multipliers technique. For that, we need to find the minimum of the function

$$F(q_X, q_Y, \lambda) = D_{XY}(q_X, q_Y) - \lambda \cdot (q_X + q_Y - Q)$$

with respect to variables q_X, q_Y, and of the Lagrangian multiplier λ. This is done by solving the following three equations

$$\begin{cases} \frac{\partial F}{\partial q_X} = \chi_X + 2\eta_X q_X - \lambda = 0 \\ \frac{\partial F}{\partial q_Y} = \chi_Y + 2\eta_Y q_Y - \lambda = 0 \\ \frac{\partial F}{\partial \lambda} = Q - q_X - q_Y = 0 \end{cases}$$

The solution of these linear equations provides us with the optimal values of the fragments' charges:

$$\begin{cases} q_X = \frac{\eta_{XY}}{\eta_X} Q + \frac{(\chi_Y - \chi_X)}{2(\eta_X + \eta_Y)} , \\ q_Y = \frac{\eta_{XY}}{\eta_X} Q + \frac{(\chi_X - \chi_Y)}{2(\eta_X + \eta_Y)} , \end{cases} \tag{8}$$

where η_{XY} is the reduced hardness of the two fragments, given by the following expression:

$$\eta_{XY} = \left(\frac{1}{\eta_X} + \frac{1}{\eta_Y} \right)^{-1} = \frac{\eta_X \cdot \eta_Y}{\eta_X + \eta_Y} \tag{9}$$

Substitution of the optimal charges (Equation 8) into the dissociation energy (Equation 6) would yield the final (and tedious) expression for the minimal energy upon dissociation of the parent P^{Q+} into fragments "X" and "Y". However, for the hydrocarbons with a persistent sp^2 hybridization of the carbon atoms (discussed in more detail in Section 3), the electronegativities of all the species can be approximated to be the same, i.e., $\chi_P \approx \chi_X \approx \chi_Y$. This simplifies the final equation for the minimal dissociation energy of the parent cation with charge Q into fragments "X" and "Y" to be:

$$D_{XY}(Q) = D - \overbrace{(\eta_P - \eta_{XY})}^{\Delta\eta} Q^2 = D - \Delta\eta \cdot Q^2 . \tag{10}$$

The behavior of $D_{XY}(Q)$ with an increase of the charge Q depends on the sign of $\Delta\eta$. To determine it, we need to know if the hardness of the neutral parent ("P") or the reduced hardness of the neutral fragments ("X" and "Y") is larger. From Equation 5, we know that the hardness is half of the HOMO-LUMO gap of the neutral molecule, which means that the hardness should be a positive number ($\eta > 0$). Furthermore, the HOMO-LUMO gap usually tends to decrease with increasing size of the molecular system. This means that the fragments would have equal or greater hardness compared to the parent ($\eta_X, \eta_Y \geq \eta_P$). This inequality leads us to (see Equation 9)

$$\frac{1}{\eta_{XY}} = \overbrace{\frac{1}{\eta_X}}^{\leq 1/\eta_P} + \overbrace{\frac{1}{\eta_Y}}^{\leq 1/\eta_P} \leq \frac{2}{\eta_P} .$$

From here, we obtain $\eta_P \geq 2\eta_{XY}$, which means that $\Delta\eta = \eta_P - \eta_{XY} \geq \eta_{XY} > 0$. Thus, with the increase of charge Q, we inevitably hit a point when the parent polycation becomes thermodynamically unstable (i.e., condition 7 will be broken).

Chemically, this result is simple to comprehend. When ionizing the parent, we remove electrons from the valence shell, which is responsible for the chemical bonds holding the molecule together. Thus, if too many electrons are removed, fragmentation will be thermodynamically preferable. Note that the parent species still might exist, but as a metastable state, protected by the activation energy for the fragmentation reaction 1. The charge at which the parent molecule will become thermodynamically unstable for fragmentation into fragments "X" and "Y" is denoted as the maximum charge $Q_{XY,max}$, which can be obtained from Equation 10 by setting $D_{XY}(Q) = 0$, giving

$$Q_{XY,max} = \sqrt{\frac{D}{\Delta\eta}} . \tag{11}$$

The limiting charge for the polycation thermodynamic stability will be the lowest one, and thus the maximal charge that the parent molecule can acquire without being prone to breakup is

$$\max(Q_P) = \min_{X,Y} \{Q_{XY,max}\} . \tag{12}$$

3 Existence of the polycations of linear and cyclic conjugated hydrocarbons

3.1 Computational details

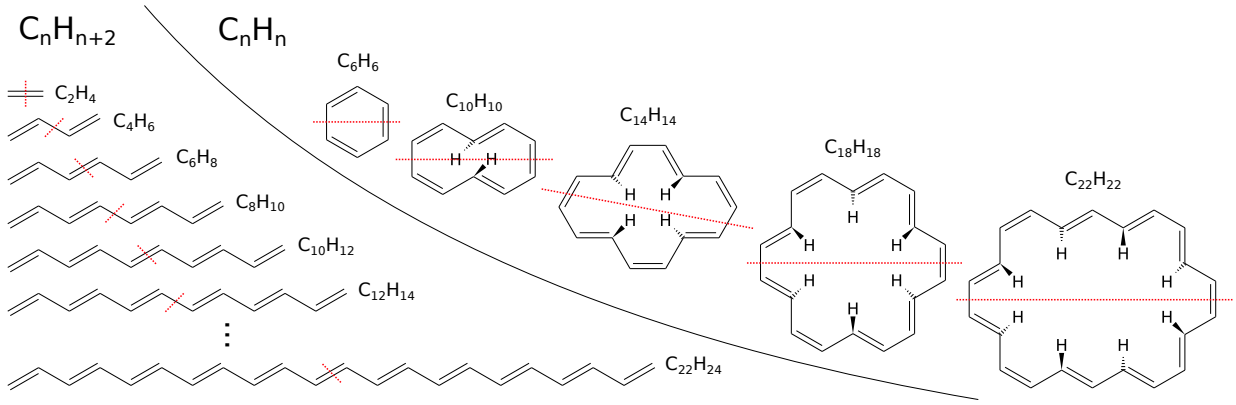

Figure 1: Linear polyenes ($C_{2n}H_{2n+2}$) and monocyclic Hückel annulenes ($C_{4n+2}H_{4n+2}$) considered in this work. The dashed red lines denote the broken bonds upon dissociation into two equivalent fragments. The justification of the equivalent fragment dissociation being the most preferable pathway is given in the Appendix.

In the following, we will treat the dissociation of the two classes of hydrocarbons with extended π-systems as examples: linear polyenes ($C_{2n}H_{2n+2}$) and monocyclic Hückel annulenes ($C_{4n+2}H_{4n+2}$), see Figure 1. We will consider the molecules up to 22 carbon atoms, comprising 11 linear polyenes ($n = 1, \ldots, 11$) and 5 annulenes ($n = 1, \ldots, 5$). For the polyenes, the all-trans conformations were taken. The computational results (structures and energies) can be found in the SI.

The quantum-chemical calculations were performed at the PBE0/def2-TZVP level of theory[37, 38] using the ORCA 5 program package.[39] Each molecule was optimized in the singlet neutral state, and the harmonic frequencies were computed to confirm that the structure found is indeed a local minimum. Then, for each molecule, at the optimized neutral geometry, the energies of the doublet monoanion[1] and polycations up to pentacations were computed. Based on these optimized neutral geometries, the fragmentation products were obtained by breaking the central carbon-carbon bonds (see Figure 1). The geometries of these products, to reduce computational expenses, were not optimized. In general, this should lead to an underestimation of the dissociation energy in each case of fragmentation. However, our numerical tests for ethylene, trans-1,3-butadiene, and all-trans-1,3,5-hexatriene show that the values obtained with such approximation are well correlated with the adiabatic dissociation energies (see SI sections 1.2 and 1.3 for details).

Two multiplicities for the parent's cations and each fragment species were tested: singlet and triplet for the even and doublet and quadruplet for the odd number of electrons. For each of these species, the state with the lower energy was then chosen to calculate the ionization potentials, electron affinities (for parent species), and dissociation energies of the different neutral and cationic states.

3.2 Analytical solution using Hückel's method

HOMO and LUMO orbitals for the extended neutral π-systems are π-orbitals in the chosen system set. Therefore, we can apply Hückel's method to express the MO energies $\varepsilon_{\mathrm{HOMO}}$ and $\varepsilon_{\mathrm{LUMO}}$ as a function of the number of atoms.[36, 40]

3.2.1 Linear polyenes

In a linear polyene of K carbon atoms, each of the atoms provides one p_z orbital to form the π-system, therefore producing K MOs with energies[40]

$$\varepsilon_k = \alpha + 2\beta \cos\left(\frac{\pi \cdot k}{K+1}\right) , \tag{13}$$

where $k = 1, 2, \ldots, K$ enumerates the π-orbitals, and parameters $\alpha, \beta \leq 0$ denote the energy of the unperturbed p_z orbital (α) and coupling between neighbouring p_z orbitals (β). For a neutral linear polyene of K carbon atoms, the

[1] Monoanions were computed to obtain the EA values.

HOMO's orbital number will be $k_{\mathrm{HOMO}} = \frac{K}{2}$, therefore[2]

$$\varepsilon_{\mathrm{HOMO}} = \varepsilon_{K/2} = \alpha + 2\beta\cos\left(\frac{\pi K}{2(K+1)}\right) = \alpha + 2\beta\sin\left(\frac{\pi}{2}\frac{1}{(K+1)}\right) \approx \alpha + \frac{\pi\beta}{K+1} \ .$$

Similarly, the LUMO's number is $k_{\mathrm{LUMO}} = \frac{K}{2} + 1$, and thus

$$\varepsilon_{\mathrm{LUMO}} = \varepsilon_{(K/2)+1} = \alpha + 2\beta\cos\left(\frac{\pi K}{2(K+1)} + \frac{\pi}{(K+1)}\right) = \alpha - 2\beta\sin\left(\frac{\pi}{2}\frac{1}{(K+1)}\right) \approx \alpha - \frac{\pi\beta}{K+1}$$

Using Koopmans' theorem, we can re-parametrize these expressions. The IP for the K-carbon linear polyene is

$$\mathrm{IP}_K = -\varepsilon_{\mathrm{HOMO}} \approx -\alpha - \frac{\pi\beta}{(K+1)} = \mathrm{IP}_\infty + \frac{B}{K+1} \ , \tag{14}$$

where both parameters $\mathrm{IP}_\infty = -\alpha$ and $B = -\pi\beta$ are non-negative (unlike the original α and β). This gives us

$$\begin{cases} \varepsilon_{\mathrm{HOMO}} = -\mathrm{IP}_\infty - \frac{B}{K+1} \\ \varepsilon_{\mathrm{LUMO}} = -\mathrm{IP}_\infty + \frac{B}{K+1} \end{cases} .$$

With these expressions, we can rewrite the χ and η (Equations 4 and 5) for the linear polyene of K-carbons as follows. The electronegativity is

$$\chi_K = \mathrm{IP}_\infty \geq 0 \ , \tag{15}$$

which means that it does not depend on the size of the polyene's chain and also that the energy of the molecule (Equation 3) increases upon ionization. For the hardness, the final expression is

$$\eta_K = \frac{B}{K+1} \geq 0 \ , \tag{16}$$

therefore, the hardness in this model (which is also half of the HOMO-LUMO gap, see Equation 5) approaches zero when increasing the size of the molecule.

Upon the dissociation of the linear polyene of N carbon atoms *via* the carbon-carbon bond cleavage following the reaction

$$\overbrace{\mathrm{C}_N\mathrm{H}_{N+2}^{Q+}}^{\mathrm{P}^{Q+}} \rightarrow \overbrace{\mathrm{C}_{N_\mathrm{X}}\mathrm{H}_{M_\mathrm{X}}^{q_\mathrm{X}+}}^{\mathrm{X}^{q_\mathrm{X}+}} + \overbrace{\mathrm{C}_{N_\mathrm{Y}}\mathrm{H}_{M_\mathrm{Y}}^{q_\mathrm{Y}+}}^{\mathrm{Y}^{q_\mathrm{Y}+}}$$

two polyenes of smaller sizes are formed; therefore, their hardness will also be given by equation 16. This means that the reduced hardness of the products (Equation 9) will be

$$\eta_{XY} = \frac{B}{N+2} \ . \tag{17}$$

Note that in Hückel's method, the reduced hardness does not depend on the size of the fragments, i.e., all fragmentation channels are equivalent. Substituting this equation and $\eta_\mathrm{P} = \frac{B}{N+1}$ (Equation 16) into the equation 11 gives maximal charge of the linear polyene as

$$Q_{\max} = \sqrt{\frac{D_{\mathrm{poly}}}{B}(N+2)(N+1)} \ , \tag{18}$$

where D_{poly} is the dissociation energy of the neutral polyene.

3.2.2 Cyclic annulenes

Let us now assume that we have a monocyclic annulene $\mathrm{C}_N\mathrm{H}_N^{Q+}$ with charge Q. We want to know the dissociation energy of the backbone of this cation into two smaller charged linear polyene fragments $\mathrm{X} = \mathrm{C}_{N_\mathrm{X}}\mathrm{H}_{N_\mathrm{X}}^{q_\mathrm{X}+}$ and $\mathrm{Y} = \mathrm{C}_{N_\mathrm{Y}}\mathrm{H}_{N_\mathrm{Y}}^{q_\mathrm{Y}+}$ with charges q_X and q_Y, respectively. This corresponds to the energy of the chemical reaction:

$$\overbrace{\mathrm{C}_N\mathrm{H}_M^{Q+}}^{\mathrm{P}^{Q+}} \rightarrow \overbrace{\mathrm{C}_{N_\mathrm{X}}\mathrm{H}_{N_\mathrm{X}}^{q_\mathrm{X}+}}^{\mathrm{X}^{q_\mathrm{X}+}} + \overbrace{\mathrm{C}_{N_\mathrm{Y}}\mathrm{H}_{N_\mathrm{Y}}^{q_\mathrm{Y}+}}^{\mathrm{X}^{q_\mathrm{X}+}} \ . \tag{19}$$

As before, both charge and number of atoms must be conserved, i.e., $N = N_\mathrm{X} + N_\mathrm{Y}$ and $Q = q_\mathrm{X} + q_\mathrm{Y}$.

[2] We use $\frac{\pi K}{2(K+1)} = \frac{\pi}{2} - \frac{\pi}{2}\frac{1}{(K+1)}$ and $\sin(x) \approx x$ for small x.

The derivation of the charge-size relation will be similar to linear polyenes in the previous section. As the values for the dissociation products (linear polyenes) are already known (Equations 15 and 16), that leaves the electronegativity and hardness of the parent species to be determined.

The MO energies of the cyclic polyenes within the same Hückel approximation are given by the following equation:[40]

$$\varepsilon_k = \alpha + 2\beta \cos\left(\frac{2\pi k}{N}\right) \ , \tag{20}$$

where $k = 0, \pm1, \pm2, \ldots, \pm\frac{(N-1)}{2}, \frac{N}{2}$ for even N, and $k = 0, \pm1, \pm2, \ldots, \pm\frac{(N-1)}{2}$ for odd N. Each MO is doubly degenerate, except for $k \neq 0$ and $k \neq N/2$ (for even N), which means that $\varepsilon_k = \varepsilon_{-k}$, and that the energy of the MO increases with an increase of $|k|$. The $|k|$ is essentially an MO's angular momentum quantum number. We will limit ourselves to Hückel aromatic annulenes, where $N = 4l + 2$ with $l = 0, 1, 2, \ldots$.[41] The integer number l denotes essentially the k-value of the HOMO (k_{HOMO}), which leads to $N = 4k_{\mathrm{HOMO}} + 2$. And $k_{\mathrm{LUMO}} = l + 1$, since all the $\pm k$ MOs are occupied for Hückel aromatic annulenes. We can formally rewrite $N = 4l + 2$ as $l = (N-2)/4$, which will give $k_{\mathrm{HOMO}} = (N-2)/4$ and $k_{\mathrm{LUMO}} = 1 + (N-2)/4$. Therefore, the energies of these orbitals from Equation 20 are

$$\varepsilon_{\mathrm{HOMO}} = \varepsilon_{(N-2)/4} = \alpha + 2\beta \cos\left(\frac{\pi}{2} - \frac{\pi}{N}\right) = \alpha + 2\beta \sin\left(\frac{\pi}{N}\right) \approx \overbrace{\alpha}^{-\mathrm{IP}_\infty} + \frac{2\overbrace{\beta\pi}^{-B}}{N} = -\mathrm{IP}_\infty - \frac{2B}{N} \tag{21}$$

and

$$\varepsilon_{\mathrm{LUMO}} = \varepsilon_{1+(N-2)/4} = \alpha + 2\beta \cos\left(\frac{\pi}{2} + \frac{\pi}{N}\right) = \alpha - 2\beta \sin\left(\frac{\pi}{N}\right) \approx \overbrace{\alpha}^{-\mathrm{IP}_\infty} - \frac{2\overbrace{\beta\pi}^{-B}}{N} = -\mathrm{IP}_\infty + \frac{2B}{N} \ . \tag{22}$$

Now, substituting these Equations 21 and 22 into expressions 4 and 5, we get Equation 15 for the electronegativity (χ) and

$$\eta_N = \frac{2B}{N} \tag{23}$$

The products' reduced hardness will be again given by Equation 17. Substitution of Equations 23 and 17 into Equation 11 gives us the final maximal charge of the annulene as:

$$Q_{\max} = \sqrt{\frac{D_{\mathrm{annu}}}{B} N} \ , \tag{24}$$

where D_{annu} is the dissociation energy of the neutral annulene.

3.3 Parametrization of the model

Let us look at the set of parameters obtained from the quantum-chemical calculations: IP, EA, electronegativity χ (Equation 4), hardness η (Equation 5), and also the dissociation energies of the neutral molecule into two equivalent molecular fragments according to Figure 1. The resulting trends as a function of the number of carbon atoms in the molecule are given in Figure 2. The IP decreases and EA increases with an increasing number of carbon atoms. However, their mean value (χ) remains rather constant, as predicted with Hückel's method. This means that our approximation, resulting in Equation 11, applies to this type of system.

To apply the Hückel's model expressions (Equations 18 and 24), we also need an estimation of the coupling strength of the sp^2-hybridized orbitals, given as parameter B in Equations 18 and 24. To obtain such an expression, the Equation 14 was fitted to the quantum-chemically computed values of polyenes, giving $\mathrm{IP}_\infty = 5.4 \pm 0.1$ [eV] and $B = 16.1 \pm 0.7$ [eV]. The second parameters, D_{poly} and D_{annu}, were taken as the means of the dissociation energies of the neutrals of all computed sizes. The values for both polyenes and annulenes approach some limit, therefore justifying such an operation. The oscillations of the dissociation energies for polyenes arise from the alternating middle bond being either a formally single or double bond (see Figure 1). The resulting values were $D_{\mathrm{poly}} = 6.5 \pm 0.7$ [eV] and $D_{\mathrm{annu}} = 12.3 \pm 0.5$ [eV]. Note that $D_{\mathrm{annu}} \approx 2 \times D_{\mathrm{poly}}$, because two carbon-carbon bonds are being broken during the dissociation of the annulene.

The main flaw of the Hückel's method solution is that the HOMO-LUMO gap of the extended systems decreases to zero upon increasing the size of the polyene/annulene. As we can see from quantum chemistry (Figure 2), η decreases in the case of both the polyenes and annulenes, but not to zero, as predicted by Hückel's model, but to some finite value. To remove this limitation, we use a three-parametric expression for approximating quantum-chemical values to obtain the carbon backbone length-dependent graphs:

$$\eta_N = \eta_\infty + \frac{\eta_0}{N + K} \ , \tag{25}$$

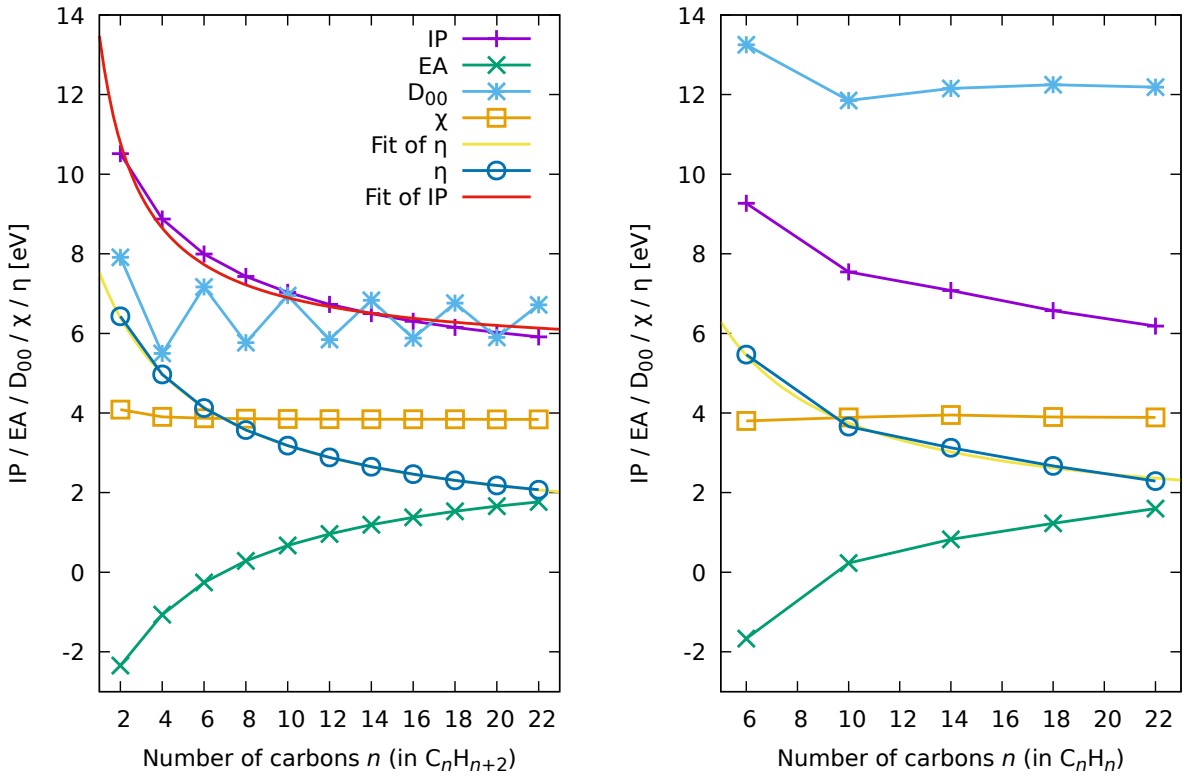

Figure 2: Ionization potentials (IP), electron affinities (EA), electronegativity (χ), hardness (η), and dissociation energies of the neutral molecule (D_{00}) of the linear polyenes (left) and monocyclic annulenes (right) as a function of the number of carbon atoms in the molecule. The IPs of polyenes were fitted with Equation 14. The legend is the same in the left and right plots.

where N is the number of carbon atoms in the molecule, and the three fitting parameters are η_∞, η_0, and K. K was limited to integer numbers. The results of the fitting are $\eta_\infty^{(\mathrm{poly})} = 0.77 \pm 0.1$ [eV], $\eta_0^{(\mathrm{poly})} = 33.8 \pm 0.1$ [eV], and $K^{(\mathrm{poly})} = 4$ for the polyenes and $\eta_\infty^{(\mathrm{annu})} = 1.2 \pm 0.1$ [eV], $\eta_0^{(\mathrm{annu})} = 25 \pm 1$ [eV], and $K^{(\mathrm{annu})} = 0$ for annulenes.

With the hardness of the form given by Equation 25, the most energetically favorable breakdown channel is dissociation into two equal fragments (see Appendix for proof). In this case, when a polyene or annulene with N carbon atoms dissociates into two polyenes with $N/2$ carbons, we get the reduced hardness (Equation 9) to be

$$\eta_{\mathrm{XY}} = \frac{\eta_{N/2}^{(\mathrm{poly})}}{2} \,,$$

where $\eta_{N/2}^{(\mathrm{poly})}$ corresponds to applying Equation 25 with $N/2$ atoms and polyene parameters, given above. We note that this assumption of symmetric dissociation may fail if stable products are formed, like in the case of acetylene–like fragments.[5] In particular, we observe this for adiabatic dissociation energies of the all-trans-1,3,5-hexatriene (section 1.3 of SI). However, the numerical tests show that the dissociation energy trends correlate well for the lowest energy asymmetric dissociation and the symmetric energy dissociation channels.

3.4 Comparison of the model with quantum chemistry

We have computed the dissociation energies for each of the charge states of the polyenes and annulenes and dissociation pathways given in Figure 1. As an example, the result is provided for the polyenes in Figure 3. We can think of the resulting map as a phase diagram in the size-maximal charge space: the positive dissociation energies correspond to thermodynamically stable polycations of a given size and charge, whether the negative ones are the thermodynamically unstable species that are prone to carbon backbone dissociation. To estimate more accurately the maximal charge at a given size for a given molecule, we can use the following approximation. First, determine the last stable integer charge Q of the molecule with dissociation energy $D(Q) \geq 0$. Then, use a linear approximation of dissociation energy

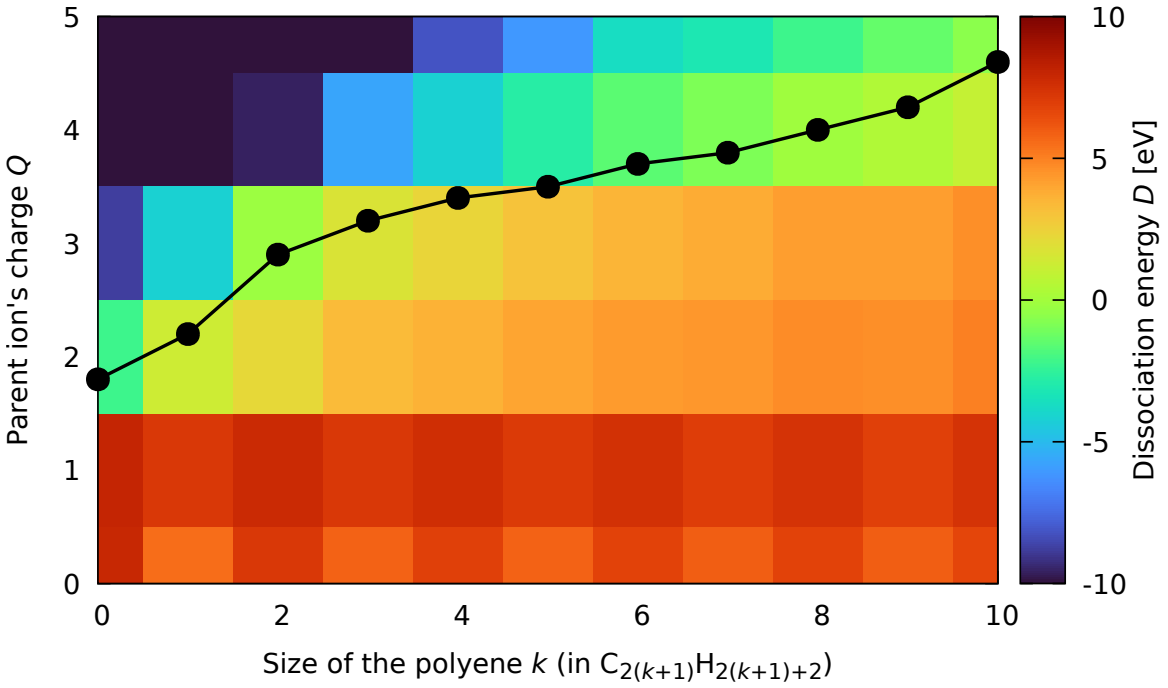

Figure 3: Dissociation energies for the linear polyenes of different sizes and cationic charge states. The black line approximates each species' maximal charge $Q_{\max}$.

D in the range of charges between Q and $Q+1$ to find the $Q_{\max}$ from condition $D(Q_{\max})=0$ as

$$Q_{\max} \approx Q + \frac{D(Q)}{D(Q) - D(Q+1)} \ .$$

The corresponding line can be considered an approximate phase-change line, and such a result for polyenes is shown in Figure 3.

Additionally, we can compare the quantum-chemically computed $Q_{\max}$ values with the quantum-chemically parameterized models, both based on simple Hückel's method and more general parametrizations with hardness given by Equation 25. The results are shown in Figure 4. The trend for the polyenes from Hückel's method is too fast-growing, which is attributed to the HOMO-LUMO gap approaching zero. The empirically-fitted hardness gives better trends, although lower in energy than the quantum-chemical values. This is probably due to approximating the parent species and using their values for the fragments. In the case of linear polyenes, this approximation gives better results since the products are reminiscent of the parent species. However, in the case of the annulene species, the resulting fragments are structurally different from those from polyenes, and these effects, like differences in trans-/cis- energies, can lead to the observed deviations. Nevertheless, we can say that the approximate model based on the hardness of the reagents and products reproduces the important features of the size-maximal charge phase diagrams.

4 Critical sizes of multicharged helium droplets

In the next step, we apply the same principles to the thermodynamic stability of the weakly bound clusters in the most straightforward example, i.e., in the case of helium clusters, for which experimental data on the critical sizes of the clusters with different charges is available from the literature. [42, 43] We also can find the expression of the helium clusters' (He_n) energies as a function of the number of atoms n:[44, 45]

$$E_{\text{tot}}(n) = -\varepsilon_\infty \cdot n + \varepsilon_{2/3} \cdot n^{2/3} - \varepsilon_{1/3} \cdot n^{1/3} \ , \tag{26}$$

where ε_∞, $\varepsilon_{2/3}$, and $\varepsilon_{1/3}$ are the fitted coefficients.

We obtained the parametrizations of the energy, electronegativity, and hardness as a function of the helium cluster size using the following procedure:

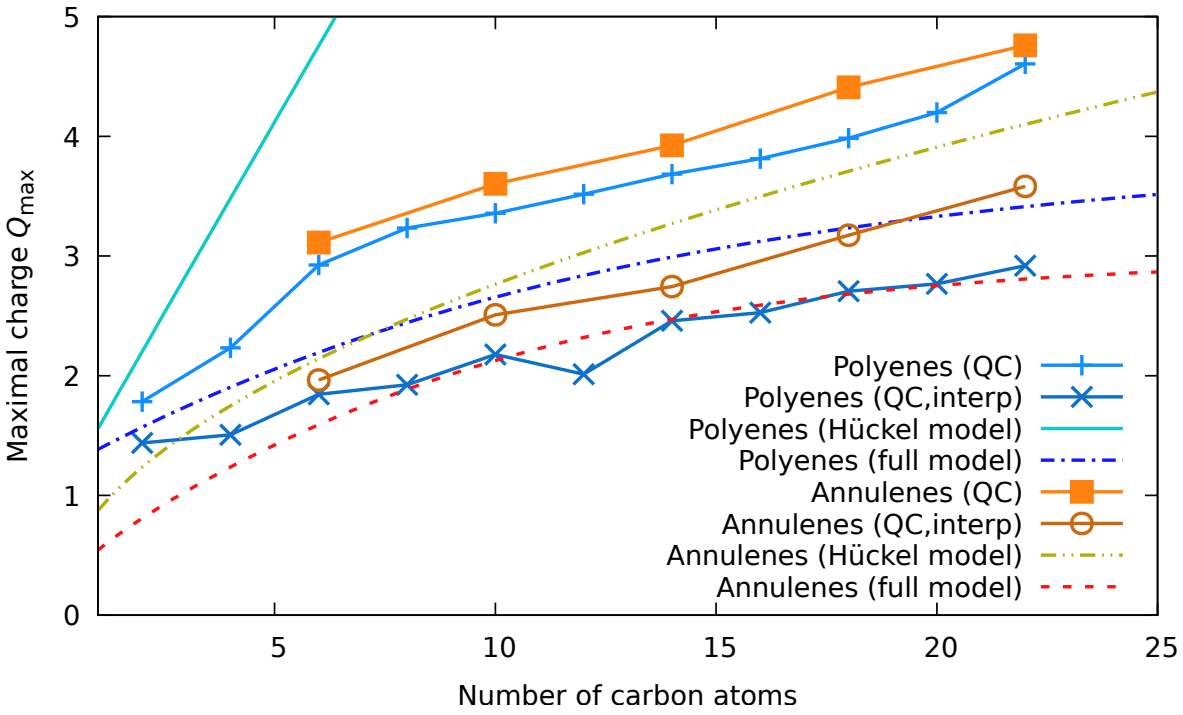

Figure 4: Maximal charge $Q_{\max}$ *vs.* molecule's size phase diagrams for linear polyenes and monocyclic annulenes. "QC" denotes the values extracted from the dissociation energies of the different species (see Figure 3), "QC,interp" denotes interpolated values using Equation 11 from the computed neutral dissociation energies and hardnesses η, "Hückel model" is the approximation based on the analytical HOMO-LUMO gaps from the Hückel model, and "full model" uses the empirically fitted HOMO-LUMO gaps according to Equation 25.

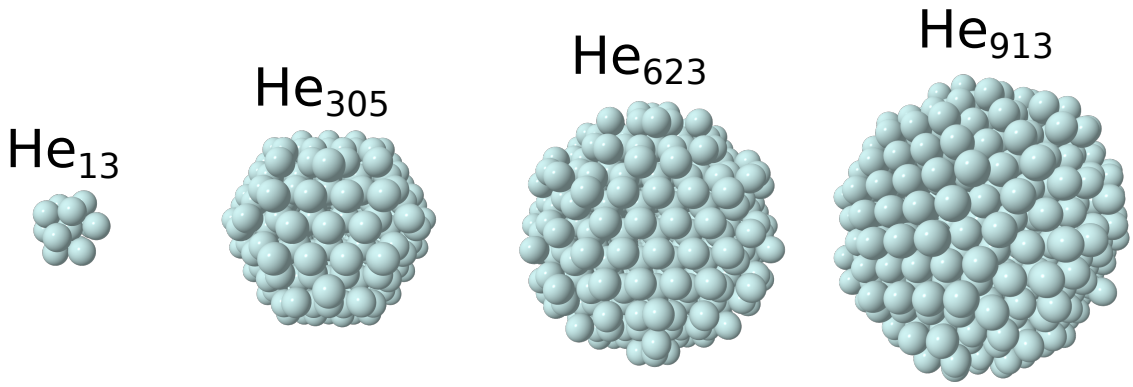

Figure 5: Examples of GFN2-xTB-optimized structures of the He_n clusters.

- Various helium cluster initial geometries for $n \leq 1000$ were cut from the hexagonal closed packing (HCP) spherical cluster of 1002 atoms, optimized using the GFN-FF force field[46] implemented in xTB software. HCP-type arrangement was chosen as a building pattern for clusters since solid helium can exist in this structure.[47] For each of these He_n clusters, structure optimization and harmonic frequency calculations were performed at the semi-empirical GFN2-xTB level of theory[48] using the xTB software.[49]

- For these He_n clusters, the single point energies ($E(n)$) were computed at the DLPNO-CCSD/aug-cc-pVDZ level of theory. IP and EA were computed using IP-EOM-DLPNO-CCSD/aug-cc-pVDZ, and EA-EOM-DLPNO-CCSD/aug-cc-pVDZ levels of theory, respectively. All these calculations were done using the ORCA 5 program package.[39]

- The resulting total energies ($E_{\text{tot}}(n) = E(n) + \text{ZPVE}$), comprised of the zero-point vibrational energy (ZPVE)

at the GFN2-xTB level of theory and the electronic energy ($E(n)$) at the DLPNO-CCSD/aug-cc-pVDZ level of theory, were fitted to the Equation 26. The resulting parameters were $\varepsilon_\infty = 78.6531 \pm 0.0001$ [eV], $\varepsilon_{2/3} = 13.8 \pm 0.6$ [meV], and $\varepsilon_{1/3} = 11.2 \pm 0.5$ [meV].

- The IPs and EAs were then fitted to the equations

$$\begin{cases} \mathrm{IP}(n) = \mathrm{IP}_\infty + \mathrm{IP}_0 \cdot n^{-1/3} \ , \\ \mathrm{EA}(n) = \mathrm{EA}_\infty + \mathrm{EA}_0 \cdot n^{-1/3} \ , \end{cases} \tag{27}$$

with these parameters being $\mathrm{IP}_\infty = 24.066 \pm 0.004$ [eV], $\mathrm{IP}_0 = 0.32 \pm 0.01$ [eV], $\mathrm{EA}_\infty = -4.12 \pm 0.03$ [eV], $\mathrm{EA}_0 = -0.6 \pm 0.1$ [eV]. These trends were then corrected for the experimental values of IP and EA for the helium atom ($\mathrm{IP}_{\mathrm{exp}}(\mathrm{He}) = 24.6$ [eV] and $\mathrm{EA}_{\mathrm{exp}}(\mathrm{He}) = 0.1$ [eV])[50, 51] by adding corrections $\mathrm{IP}_{\mathrm{corr}} = \mathrm{IP}_{\mathrm{exp}}(\mathrm{He}) - \mathrm{IP}(1) = 0.2$ [eV] and $\mathrm{EA}_{\mathrm{corr}} = \mathrm{EA}_{\mathrm{exp}}(\mathrm{He}) - \mathrm{EA}(1) = 4.7$ [eV].

- From the corrected IP and EA dependencies (Equation 27), we produce the approximations for χ and η for He_n clusters according to Equations 4 and 5:

$$\begin{cases} \chi(n) = (\mathrm{IP}(n) + \mathrm{EA}(n) + \mathrm{IP}_{\mathrm{corr}} + \mathrm{EA}_{\mathrm{corr}})/2 = \chi_\infty + \chi_0 \cdot n^{-1/3} \ , \\ \eta(n) = (\mathrm{IP}(n) - \mathrm{EA}(n) + \mathrm{IP}_{\mathrm{corr}} - \mathrm{EA}_{\mathrm{corr}})/2 = \eta_\infty + \eta_0 \cdot n^{-1/3} \ , \end{cases} \tag{28}$$

where, from Equation 27, we get

$$\begin{cases} \chi_\infty = (\mathrm{IP}_\infty + \mathrm{EA}_\infty + \mathrm{IP}_{\mathrm{corr}} + \mathrm{EA}_{\mathrm{corr}})/2 = 12.4 \text{ [eV]} \ , \\ \chi_0 = (\mathrm{IP}_0 + \mathrm{EA}_0)/2 = -0.1 \text{ [eV]} \ , \\ \eta_\infty = (\mathrm{IP}_\infty - \mathrm{EA}_\infty + \mathrm{IP}_{\mathrm{corr}} - \mathrm{EA}_{\mathrm{corr}})/2 = 11.8 \text{ [eV]} \ , \\ \eta_0 = (\mathrm{IP}_0 - \mathrm{EA}_0)/2 = 0.4 \text{ [eV]} \ . \end{cases} \tag{29}$$

A detailed description of this procedure, justification of the methods used, and numerical results are available in the SI (Section 2).

Unlike in the covalently bound molecules discussed above (polyenes and annulenes), the change in electronegativity of the helium clusters (He_n) is noticeable upon increasing cluster size. Therefore, Equation 11 is insufficient due to negligence of the change in χ. To account for that, let us reevaluate the solution. First, we examine the optimal charges of the fragments in Equation 8. The maximal value of the Q-independent term for the helium clusters can be estimated as (see Equations 28 and 29)

$$\left| \frac{\chi_\mathrm{X} - \chi_\mathrm{Y}}{2(\eta_\mathrm{X} + \eta_\mathrm{Y})} \right| \leq \frac{|\chi_0|}{4\eta_\infty} = 0.002 \ .$$

From this estimation, we can neglect this Q-independent term in Equation 8, giving us approximate optimal charges that do not account for spontaneous charge separation upon neutral dissociation:

$$\begin{cases} q_\mathrm{X} \approx \frac{\eta_\mathrm{Y} Q}{\eta_\mathrm{X} + \eta_\mathrm{Y}}, \\ q_\mathrm{Y} \approx \frac{\eta_\mathrm{X} Q}{\eta_\mathrm{X} + \eta_\mathrm{Y}}, \end{cases}$$

and their substitution into the dissociation energy (Equation 6) gives the equation for obtaining the maximal stable charge

$$D - \Delta\chi Q - \Delta\eta Q^2 = 0 \ , \tag{30}$$

where $\Delta\eta$ is given by the same expression from Equation 10, and $\Delta\chi$ is defined as

$$\Delta\chi = \chi_\mathrm{P} - \left(\frac{\eta_\mathrm{Y}\chi_\mathrm{X}}{\eta_\mathrm{X} + \eta_\mathrm{Y}} + \frac{\eta_\mathrm{X}\chi_\mathrm{Y}}{\eta_\mathrm{X} + \eta_\mathrm{Y}} \right) \ . \tag{31}$$

Equations 28 and 29 show that with increasing size, the electronegativity also increases. Thus, $\chi_\mathrm{P} \geq \chi_\mathrm{X}, \chi_\mathrm{Y}$. Assuming that $\chi_\mathrm{X} \geq \chi_\mathrm{Y}$, we get

$$\frac{\eta_\mathrm{Y}\chi_\mathrm{X}}{\eta_\mathrm{X} + \eta_\mathrm{Y}} + \frac{\eta_\mathrm{X} \overbrace{\chi_\mathrm{Y}}^{\leq \chi_\mathrm{X}}}{\eta_\mathrm{X} + \eta_\mathrm{Y}} \leq \chi_\mathrm{X} \leq \chi_\mathrm{P} \ ,$$

thus $\Delta\chi \geq 0$. Solving Equation 30, we obtain the final expression:

$$Q_{\max} = -\frac{\Delta\chi}{2\Delta\eta} + \frac{1}{2\Delta\eta}\sqrt{\Delta\chi^2 + 4\Delta\eta \cdot D} \ . \tag{32}$$

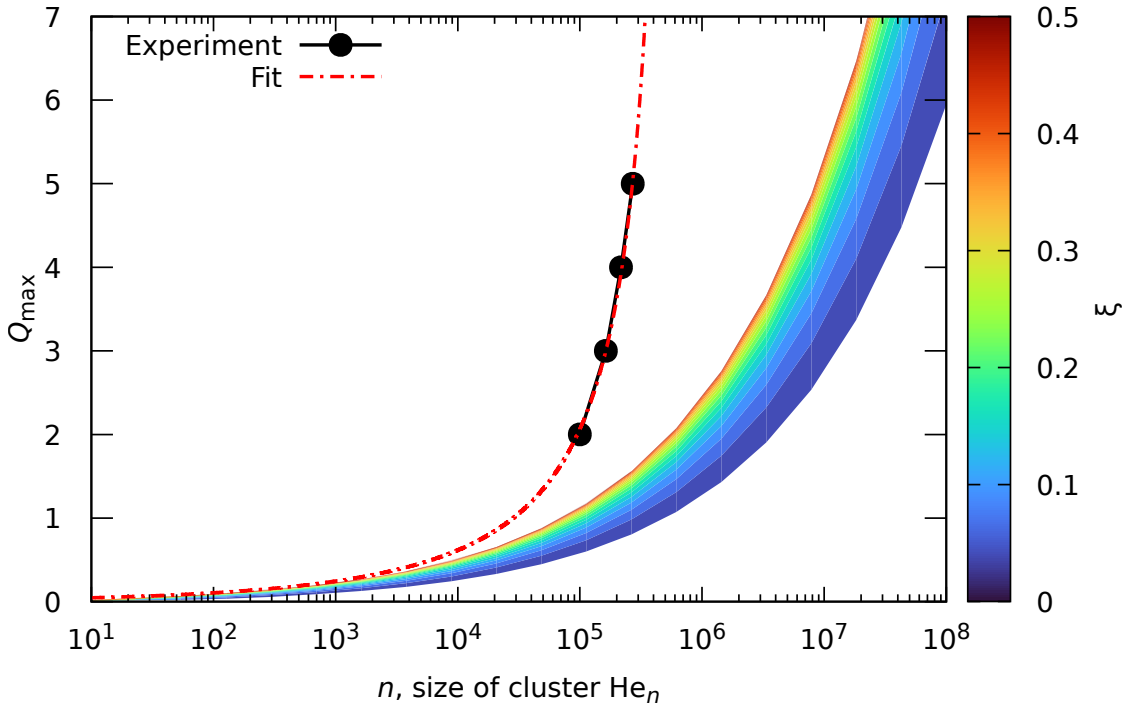

Figure 6: Experimental (points)[42] and model (colored area) maximal possible charge of helium clusters as a function of cluster size. ξ is the asymmetry parameter for the dissociation reaction (Equation 34). The "Fit" curve represents the fit of the experimental points to Equation 32 (see main text for details).

Unlike the previously discussed cases of polyenes and annulenes, all three parameters ($\Delta\chi$, $\Delta\eta$, and D) are size-dependent for the helium clusters.

For evaluating the stability of the charged helium clusters, we evaluate the dissociation according to the reaction

$$\mathrm{He}_n^{Q+} \rightarrow \mathrm{He}_{n_x}^{Q_x+} + \mathrm{He}_{n_y}^{Q_y+} \ , \ (Q_x + Q_y = Q, \ n_x + n_y = n, \ n_x \geq n_y) \ . \tag{33}$$

To characterize the asymmetry of the large cluster breakup, we introduce a parameter $\xi \in (0, 1/2]$ defined as

$$\xi = \frac{n_y}{n} \ , \tag{34}$$

where symmetric breakup $n_x = n_y = n/2$ corresponds to $\xi = 1/2$, and maximally asymmetric breakup $n_x = n - 1$, $n_y = 1$ is denoted by $\xi = 1/n$.

The results of Equation 32 with parameters D, $\Delta\chi$, and $\Delta\eta$ computed from parametrized Equations 26 and 28 are also included in Figure 6. If we compare our results with the experimental data,[42, 43] we see very similar trends of increasing stability of the poly-charged helium clusters with the increase of cluster size. It is worth noting that, unlike the polyenes and annulenes, helium clusters are more stable for the symmetric breakup ($\xi = 1/2$) than for the small cluster removal ($\xi \rightarrow 0$). This is in agreement with the experimental observations, where the strong evaporation of charged helium clusters was observed via the removal of small charged fragments and not through symmetric Coulomb explosions.[43]

Despite the qualitative agreement of our theoretically predicted stability trends with the experimental observations, the quantitative predictions differ from the actual observed trends. The main reason for this is that our theoretical methodology has a limited quality of the quantum-chemical calculations, in particular for the sampling of the conformational space, poor harmonic approximation of the ZPVE for the superfluid vibrational state,[44] limited size of the basis set for calculation of the electronic energies, and significant failures of the conventional basis sets to describe the EA of helium (see SI for details). These defects of the theoretical model, combined with extrapolation of the parameters from cluster size ranges of $1 \leq n < 1000$ up to $n \sim 10^8$, can lead to significant deviations in the observed trends.

To align the model and experiment, we fitted the parameters of our model to the experimental data. The expression for the $Q_{\max}$ (Equation 32) was fitted to the observed experimental trend by varying parameters from Equations 29, that are used in Equations 28. A fit for χ and η included only a single parameter, with $\chi(1)$ and $\eta(1)$ being taken

from the experimental IP and EA values of the helium atom. The energy expression (Equation 26) was taken with parameters from the literature, namely $\varepsilon_\infty = 0.621$ [meV], $\varepsilon_{2/3} = 1.526$ [meV], and $\varepsilon_{1/3} = 0.513$ [meV].[44, 45] Due to numerical instabilities of the fit, the smallest possible $\xi = 0.4$ was taken. The fitting resulted in a curve reproducing the observations, as can be seen from Figure 6. This shows the potential of the proposed model for describing experimental observations.

5 Conclusions

Here, we provided a new approach for computing the maximal possible charge a molecular polycation can carry without being thermodynamically unstable ($Q_{\max}$). The approach is based on the quadratic approximation of the ionization potentials using the energy expansion in terms of Mulliken's electronegativity and Pearson's hardness. For the conjugated hydrocarbons, $Q_{\max}$ can be estimated using Equation 11, and the value for the molecule is provided as the lowest of those values for different fragmentation pathways. This estimation reduced the computations to calculations of only the molecule's and fragment's electronic energy, ionization potential, and electron affinity. Further, by parametrizing these properties with some molecular descriptors, one can produce analytical approximations for the maximal charges, which is essentially a phase diagram of the thermodynamic stability of molecular polycations. We demonstrated the applicability and efficiency of this approach using the three model systems: linear polyenes, monocyclic annulenes, and helium clusters.

The resulting approach can be useful in the field of astrochemistry to produce effective and sufficiently accurate approximations for quasi-thermodynamic modeling of the interstellar medium, interplanetary environment, and atmospheres of exoplanets, to include the possibility of polycationic states in the photochemistry of molecules and molecular clusters under the influence of harsh radiation. As a perspective, the proposed approach can be extended to include the higher-order terms of the energy expansion (Equation 3), vibrational effects, and reach a more accurate approximation of thermodynamic potentials (enthalpy, entropy, free energies).

Appendix

Here, we will provide explicit proof that for the fragmentation reaction with a fixed dissociation energy and size-dependent hardness given by Equation 25, the most energetically favorable fragmentation channel for a polycation is dissociation into two equal fragments.

Equation 12 is fulfilled if $\Delta\eta = \eta_{\mathrm{P}} - \eta_{\mathrm{XY}}$ is maximal (see Equations 11 and 10), and since D and η_{P} are fixed, which is achieved by minimization of η_{XY} with respect to the fragments' sizes X and $Y = N - X$. We will take η of the fragments to depend on the sizes of fragments "X" and "Y" (x and $y = N - x$) as a function $\eta = \eta(n)$, where $\eta_{\mathrm{X}} = \eta(x)$ and $\eta_{\mathrm{Y}} = \eta(y) = \eta(N - x)$. This means, that η_{XY} (Equation 9) is given as

$$\eta_{XY}(x) = \frac{\eta(x) \cdot \eta(N-x)}{\eta(x) + \eta(N-x)} \ .$$

The stationary point of this function is found through the following equation:

$$\frac{d\eta_{XY}}{dx} = \eta'_{\mathrm{XY}} = \frac{\eta'(x) \cdot \eta^2(N-x) - \eta'(N-x)' \cdot \eta^2(x)}{(\eta(x) + \eta(N-x))^2} = 0 \ ,$$

with a trivial solution $x = N/2$. To prove that the found solution is indeed a minimum, we calculate the second derivative at this point, which is given as

$$\frac{d^2\eta_{XY}}{dx^2}(N/2) = \eta''_{\mathrm{XY}}(N/2) = \frac{\eta''(N/2) \cdot \eta(N/2) - 2\left(\eta'(N/2)\right)^2}{2\eta(N/2)} \ .$$

The condition for minimum is $\eta''_{\mathrm{XY}}(N/2) > 0$, and if we check the second derivative for the Equation 25, we get

$$\eta''_{\mathrm{XY}}(N/2) = \frac{\eta_0\eta_\infty}{(N/2+K)^2(\eta_\infty(N/2+K)+\eta_0)} > 0 \ ,$$

if $\eta_0, \eta_\infty > 0$.

Conflict of interest

There are no conflicts to declare.

Acknowledgements

We acknowledge DESY (Hamburg, Germany), a member of the Helmholtz Association HGF. Quantum-chemical calculations were enabled through the Maxwell computational resources operated at Deutsches Elektronen-Synchrotron DESY, Hamburg, Germany.

References

[1] Michel Guélin and Jose Cernicharo. Organic Molecules in Interstellar Space: Latest Advances. *Frontiers in Astronomy and Space Sciences*, 9, 2022. ISSN 2296-987X. doi: 10.3389/fspas.2022.787567. URL https://www.frontiersin.org/articles/10.3389/fspas.2022.787567.

[2] A.G.G.M. Tielens. Interstellar Polycyclic Aromatic Hydrocarbon Molecules. *Annual Review of Astronomy and Astrophysics*, 46(1):289–337, 2008. doi: 10.1146/annurev.astro.46.060407.145211. URL https://doi.org/10.1146/annurev.astro.46.060407.145211.

[3] Thiago Monfredini, Heidy M Quitián-Lara, Felipe Fantuzzi, Wania Wolff, Edgar Mendoza, Alexsandre F Lago, Dinalva A Sales, Miriani G Pastoriza, and Heloisa M Boechat-Roberty. Destruction and multiple ionization of PAHs by X-rays in circumnuclear regions of AGNs. *Monthly Notices of the Royal Astronomical Society*, 488(1): 451–469, 2019. ISSN 0035-8711. doi: 10.1093/mnras/stz1021. URL https://doi.org/10.1093/mnras/stz1021.

[4] A. G. G. M. Tielens. The molecular universe. *Rev. Mod. Phys.*, 85:1021–1081, 2013. doi: 10.1103/RevModPhys.85.1021. URL https://link.aps.org/doi/10.1103/RevModPhys.85.1021.

[5] J. W. L. Lee, D. S. Tikhonov, P. Chopra, S. Maclot, A. L. Steber, S. Gruet, F. Allum, R. Boll, X. Cheng, S. Düsterer, B. Erk, D. Garg, L. He, D. Heathcote, M. Johny, M. M. Kazemi, H. Köckert, J. Lahl, A. K. Lemmens, D. Loru, R. Mason, E. Müller, T. Mullins, P. Olshin, C. Passow, J. Peschel, D. Ramm, D. Rompotis, N. Schirmel, S. Trippel, J. Wiese, F. Ziaee, S. Bari, M. Burt, J. Küpper, A. M. Rijs, D. Rolles, S. Techert, P. Eng-Johnsson, M. Brouard, C. Vallance, B. Manschwetus, and M. Schnell. Time-resolved relaxation and fragmentation of polycyclic aromatic hydrocarbons investigated in the ultrafast XUV-IR regime. *Nature Communications*, 12(1):6107, 2021. ISSN 2041-1723. doi: 10.1038/s41467-021-26193-z. URL https://doi.org/10.1038/s41467-021-26193-z.

[6] D. Garg, J. W. L. Lee, D. S. Tikhonov, P. Chopra, A. L. Steber, A. K. Lemmens, B. Erk, F. Allum, R. Boll, X. Cheng, S. Düsterer, S. Gruet, L. He, D. Heathcote, M. Johny, M. M. Kazemi, H. Köckert, J. Lahl, D. Loru, S. Maclot, R. Mason, E. Müller, T. Mullins, P. Olshin, C. Passow, J. Peschel, D. Ramm, D. Rompotis, S. Trippel, J. Wiese, F. Ziaee, S. Bari, M. Burt, J. Küpper, A. M. Rijs, D. Rolles, S. Techert, P. Eng-Johnsson, M. Brouard, C. Vallance, B. Manschwetus, and M. Schnell. Fragmentation Dynamics of Fluorene Explored Using Ultrafast XUV-Vis Pump-Probe Spectroscopy. *Frontiers in Physics*, 10, 2022. ISSN 2296-424X. doi: 10.3389/fphy.2022.880793. URL https://www.frontiersin.org/articles/10.3389/fphy.2022.880793.

[7] Junfeng Zhen, Sarah Rodriguez Castillo, Christine Joblin, Giacomo Mulas, Hassan Sabbah, Alexandre Giuliani, Laurent Nahon, Serge Martin, Jean-Philippe Champeaux, and Paul M. Mayer. VUV PHOTO-PROCESSING OF PAH CATIONS: QUANTITATIVE STUDY ON THE IONIZATION VERSUS FRAGMENTATION PROCESSES. *The Astrophysical Journal*, 822(2):113, 2016. doi: 10.3847/0004-637X/822/2/113. URL https://dx.doi.org/10.3847/0004-637X/822/2/113.

[8] Theodore P. Snow, Valery Le Page, Yeghis Keheyan, and Veronica M. Bierbaum. The interstellar chemistry of PAH cations. *Nature*, 391(6664):259–260, 1998. ISSN 1476-4687. doi: 10.1038/34602. URL https://doi.org/10.1038/34602.

[9] Ian W. M. Smith. *Ion-Neutral Reaction*, pages 1255–1259. Springer Berlin Heidelberg, Berlin, Heidelberg, 2015. ISBN 978-3-662-44185-5. doi: 10.1007/978-3-662-44185-5_807. URL https://doi.org/10.1007/978-3-662-44185-5_807.

[10] Károly Vékey. Multiply charged ions. *Mass Spectrometry Reviews*, 14(3):195–225, 1995. doi: https://doi.org/10.1002/mas.1280140304. URL https://analyticalsciencejournals.onlinelibrary.wiley.com/doi/abs/10.1002/mas.1280140304.

[11] G W Burdick, J R Appling, and T F Moran. Stable multiply charges molecular ions. *Journal of Physics B: Atomic and Molecular Physics*, 19(5):629, 1986. doi: 10.1088/0022-3700/19/5/021. URL https://dx.doi.org/10.1088/0022-3700/19/5/021.

[12] Stefano Falcinelli and Marzio Rosi. Production and Characterization of Molecular Dications: Experimental and Theoretical Efforts. *Molecules*, 25(18), 2020. ISSN 1420-3049. doi: 10.3390/molecules25184157. URL https://www.mdpi.com/1420-3049/25/18/4157.

[13] P. Rousseau, A. Ławicki, A.I.S. Holm, M. Capron, R. Maisonny, S. Maclot, E. Lattouf, H.A.B. Johansson, F. Seitz, A. Méry, J. Rangama, H. Zettergren, S. Rosén, H.T. Schmidt, J.-Y. Chesnel, A. Domaracka, B. Manil, L. Adoui, H. Cederquist, and B.A. Huber. Low-energy ions interacting with anthracene molecules and clusters. *Nuclear Instruments and Methods in Physics Research Section B: Beam Interactions with Materials and Atoms*, 279:140–143, 2012. ISSN 0168-583X. doi: https://doi.org/10.1016/j.nimb.2011.10.050. URL https://www.sciencedirect.com/science/article/pii/S0168583X1101010X. Proceedings of the Fifth International Conference on Elementary Processes in Atomic Systems Belgrade, Serbia, 21-25 June 2011.

[14] Tomoyuki Yatsuhashi and Nobuaki Nakashima. Formation and Fragmentation of Quadruply Charged Molecular Ions by Intense Femtosecond Laser Pulses. *The Journal of Physical Chemistry A*, 114(28):7445–7452, 2010. doi: 10.1021/jp103725s. URL https://doi.org/10.1021/jp103725s. PMID: 20578764.

[15] Akihiro Kitashoji, Akimasa Fujihara, Taiki Yoshikawa, and Tomoyuki Yatsuhashi. The Smallest Aromatic Tetracation Produced in Gas Phase by Intense Femtosecond Laser Pulses. *Chemistry Letters*, 48(12):1472–1475, 2019. doi: 10.1246/cl.190667. URL https://doi.org/10.1246/cl.190667.

[16] Takashi Kawaguchi, Kosei Kitagawa, Kazuo Toyota, Masatoshi Kozaki, Keiji Okada, Nobuaki Nakashima, and Tomoyuki Yatsuhashi. Smallest Organic Tetracation in the Gas Phase: Stability of Multiply Charged Diiodoacetylene Produced in Intense Femtosecond Laser Fields. *The Journal of Physical Chemistry A*, 125(36):8014–8024, 2021. doi: 10.1021/acs.jpca.1c06390. URL https://doi.org/10.1021/acs.jpca.1c06390. PMID: 34491746.

[17] A. Ławicki, A. I. S. Holm, P. Rousseau, M. Capron, R. Maisonny, S. Maclot, F. Seitz, H. A. B. Johansson, S. Rosén, H. T. Schmidt, H. Zettergren, B. Manil, L. Adoui, H. Cederquist, and B. A. Huber. Multiple ionization and fragmentation of isolated pyrene and coronene molecules in collision with ions. *Phys. Rev. A*, 83:022704, 2011. doi: 10.1103/PhysRevA.83.022704. URL https://link.aps.org/doi/10.1103/PhysRevA.83.022704.

[18] Leo Radom, Peter M. W. Gill, and Ming Wah Wong. *Fragmentation Mechanisms for Multiply-Charged Cations*, pages 219–225. Springer US, Boston, MA, 1988. ISBN 978-1-4684-7424-4. doi: 10.1007/978-1-4684-7424-4_23. URL https://doi.org/10.1007/978-1-4684-7424-4_23.

[19] Sergio Díaz-Tendero, Manuel Alcamí, and Fernando Martín. Structure and electronic properties of highly charged C60 and C58 fullerenes. *The Journal of Chemical Physics*, 123(18):184306, 2005. ISSN 0021-9606. doi: 10.1063/1.2104467. URL https://doi.org/10.1063/1.2104467.

[20] S. Díaz-Tendero, M. Alcamí, and F. Martín. Coulomb Stability Limit of Highly Charged C_{60}^{q+} Fullerenes. *Phys. Rev. Lett.*, 95:013401, 2005. doi: 10.1103/PhysRevLett.95.013401. URL https://link.aps.org/doi/10.1103/PhysRevLett.95.013401.

[21] Henning Zettergren, Goar Sánchez, Sergio Díaz-Tendero, Manuel Alcamí, and Fernando Martín. Theoretical study of the stability of multiply charged C70 fullerenes. *The Journal of Chemical Physics*, 127(10):104308, 2007. ISSN 0021-9606. doi: 10.1063/1.2768361. URL https://doi.org/10.1063/1.2768361.

[22] A. I. S. Holm, H. A. B. Johansson, H. Cederquist, and H. Zettergren. Dissociation and multiple ionization energies for five polycyclic aromatic hydrocarbon molecules. *The Journal of Chemical Physics*, 134(4):044301, 2011. ISSN 0021-9606. doi: 10.1063/1.3541252. URL https://doi.org/10.1063/1.3541252.

[23] Denis S. Tikhonov, Amlan Datta, Pragya Chopra, Amanda L. Steber, Bastian Manschwetus, and Melanie Schnell. Approaching black-box calculations of pump-probe fragmentation dynamics of polyatomic molecules. *Zeitschrift für Physikalische Chemie*, 234(7-9):1507–1531, 2020. doi: doi:10.1515/zpch-2020-0009. URL https://doi.org/10.1515/zpch-2020-0009.

[24] Ewa Erdmann, Néstor F. Aguirre, Suvasthika Indrajith, Jacopo Chiarinelli, Alicja Domaracka, Patrick Rousseau, Bernd A. Huber, Paola Bolognesi, Robert Richter, Lorenzo Avaldi, Sergio Díaz-Tendero, Manuel Alcamí, and Marta Łabuda. A general approach to study molecular fragmentation and energy redistribution after an ionizing event. *Phys. Chem. Chem. Phys.*, 23:1859–1867, 2021. doi: 10.1039/D0CP04890A. URL http://dx.doi.org/10.1039/D0CP04890A.

[25] Ewa Erdmann, Marta Łabuda, Néstor F. Aguirre, Sergio Díaz-Tendero, and Manuel Alcamí. Furan Fragmentation in the Gas Phase: New Insights from Statistical and Molecular Dynamics Calculations. *The Journal of Physical Chemistry A*, 122(16):4153–4166, 2018. doi: 10.1021/acs.jpca.8b00881. URL https://doi.org/10.1021/acs.jpca.8b00881. PMID: 29543456.

[26] Henning Zettergren, Alicja Domaracka, Thomas Schlathölter, Paola Bolognesi, Sergio Díaz-Tendero, Marta Łabuda, Sanja Tosic, Sylvain Maclot, Per Johnsson, Amanda Steber, Denis Tikhonov, Mattea Carmen Castrovilli, Lorenzo Avaldi, Sadia Bari, Aleksandar R. Milosavljević, Alicia Palacios, Shirin Faraji, Dariusz G. Piekarski, Patrick Rousseau, Daniela Ascenzi, Claire Romanzin, Ewa Erdmann, Manuel Alcamí, Janina Kopyra, Paulo Limão-Vieira, Jaroslav Kočišek, Juraj Fedor, Simon Albertini, Michael Gatchell, Henrik Cederquist, Henning T. Schmidt, Elisabeth Gruber, Lars H. Andersen, Oded Heber, Yoni Toker, Klavs Hansen, Jennifer A. Noble, Christophe Jouvet, Christina Kjær, Steen Brøndsted Nielsen, Eduardo Carrascosa, James Bull, Alessandra Candian, and Annemieke Petrignani. Roadmap on dynamics of molecules and clusters in the gas phase. *The European Physical Journal D*, 75(5):152, 2021. ISSN 1434-6079. doi: 10.1140/epjd/s10053-021-00155-y. URL https://doi.org/10.1140/epjd/s10053-021-00155-y.

[27] Jason W. L. Lee, Denis S. Tikhonov, Felix Allum, Rebecca Boll, Pragya Chopra, Benjamin Erk, Sebastian Gruet, Lanhai He, David Heathcote, Mehdi M. Kazemi, Jan Lahl, Alexander K. Lemmens, Donatella Loru, Sylvain Maclot, Robert Mason, Erland Müller, Terry Mullins, Christopher Passow, Jasper Peschel, Daniel Ramm, Amanda L. Steber, Sadia Bari, Mark Brouard, Michael Burt, Jochen Küpper, Per Eng-Johnsson, Anouk M. Rijs, Daniel Rolles, Claire Vallance, Bastian Manschwetus, and Melanie Schnell. The kinetic energy of PAH dication and trication dissociation determined by recoil-frame covariance map imaging. *Phys. Chem. Chem. Phys.*, 24: 23096–23105, 2022. doi: 10.1039/D2CP02252D. URL http://dx.doi.org/10.1039/D2CP02252D.

[28] Bilin P. Tsai and John H.D. Eland. Mass spectra and doubly charged ions in photoionization at 30.4 nm and 58.4 nm. *International Journal of Mass Spectrometry and Ion Physics*, 36(2):143–165, 1980. ISSN 0020-7381. doi: https://doi.org/10.1016/0020-7381(80)80064-7. URL https://www.sciencedirect.com/science/article/pii/0020738180800647.

[29] T. Hartman, P. N. Juranić, K. Collins, B. Reilly, N. Appathurai, and R. Wehlitz. Large Molecules Reveal a Linear Length Scaling for Double Photoionization. *Phys. Rev. Lett.*, 108:023001, 2012. doi: 10.1103/PhysRevLett.108.023001. URL https://link.aps.org/doi/10.1103/PhysRevLett.108.023001.

[30] T. Hartman, P. N. Juranić, K. Collins, B. Reilly, E. Makoutz, N. Appathurai, and R. Wehlitz. Photo-double-ionization mechanisms in aromatic hydrocarbons. *Phys. Rev. A*, 87:063403, 2013. doi: 10.1103/PhysRevA.87.063403. URL https://link.aps.org/doi/10.1103/PhysRevA.87.063403.

[31] Yang Wang, Sergio Díaz-Tendero, Manuel Alcamí, and Fernando Martín. Cage connectivity and frontier π orbitals govern the relative stability of charged fullerene isomers. *Nature Chemistry*, 7(11):927–934, 2015. ISSN 1755-4349. doi: 10.1038/nchem.2363. URL https://doi.org/10.1038/nchem.2363.

[32] Erich Hückel. Quantentheoretische Beiträge zum Benzolproblem. *Zeitschrift für Physik*, 70(3):204–286, 1931. ISSN 0044-3328. doi: 10.1007/BF01339530. URL https://doi.org/10.1007/BF01339530.

[33] C. Joblin, L. Dontot, G. A. Garcia, F. Spiegelman, M. Rapacioli, L. Nahon, P. Parneix, T. Pino, and P. Bréchignac. Size Effect in the Ionization Energy of PAH Clusters. *The Journal of Physical Chemistry Letters*, 8(15):3697–3702, 2017. doi: 10.1021/acs.jpclett.7b01546. URL https://doi.org/10.1021/acs.jpclett.7b01546. PMID: 28742357.

[34] Robert G. Parr and Ralph G. Pearson. Absolute hardness: companion parameter to absolute electronegativity. *Journal of the American Chemical Society*, 105(26):7512–7516, 1983. doi: 10.1021/ja00364a005. URL https://doi.org/10.1021/ja00364a005.

[35] Mihai V. Putz. Systematic formulations for electronegativity and hardness and their atomic scales within density functional softness theory. *International Journal of Quantum Chemistry*, 106(2):361–389, 2006. doi: https://doi.org/10.1002/qua.20787. URL https://onlinelibrary.wiley.com/doi/abs/10.1002/qua.20787.

[36] Attila Szabo and Neil S. Ostlund. *Modern Quantum Chemistry: Introduction to Advanced Electronic Structure Theory*. Dover Publications, Inc., first edition, 1996.

[37] Carlo Adamo and Vincenzo Barone. Toward reliable density functional methods without adjustable parameters: The PBE0 model. *The Journal of Chemical Physics*, 110(13):6158–6170, 1999. doi: 10.1063/1.478522. URL http://scitation.aip.org/content/aip/journal/jcp/110/13/10.1063/1.478522.

[38] Florian Weigend and Reinhart Ahlrichs. Balanced basis sets of split valence, triple zeta valence and quadruple zeta valence quality for H to Rn: Design and assessment of accuracy. *Phys. Chem. Chem. Phys.*, 7:3297–3305, 2005. doi: 10.1039/B508541A. URL http://dx.doi.org/10.1039/B508541A.

[39] Frank Neese, Frank Wennmohs, Ute Becker, and Christoph Riplinger. The ORCA quantum chemistry program package. *The Journal of Chemical Physics*, 152(22):224108, 2020. doi: 10.1063/5.0004608. URL https://doi.org/10.1063/5.0004608.

[40] Werner Kutzelnigg. What I like about Hückel theory. *Journal of Computational Chemistry*, 28(1):25–34, 2007. doi: https://doi.org/10.1002/jcc.20470. URL https://onlinelibrary.wiley.com/doi/abs/10.1002/jcc.20470.

[41] Miquel Solà. Aromaticity rules. *Nature Chemistry*, 14(6):585–590, 2022. ISSN 1755-4349. doi: 10.1038/s41557-022-00961-w. URL https://doi.org/10.1038/s41557-022-00961-w.

[42] Felix Laimer, Fabio Zappa, Paul Scheier, and Michael Gatchell. Multiply Charged Helium Droplet Anions. *Chemistry – A European Journal*, 27(25):7283–7287, 2021. doi: https://doi.org/10.1002/chem.202005004. URL https://chemistry-europe.onlinelibrary.wiley.com/doi/abs/10.1002/chem.202005004.

[43] Felix Laimer, Lorenz Kranabetter, Lukas Tiefenthaler, Simon Albertini, Fabio Zappa, Andrew M. Ellis, Michael Gatchell, and Paul Scheier. Highly Charged Droplets of Superfluid Helium. *Phys. Rev. Lett.*, 123:165301, 2019. doi: 10.1103/PhysRevLett.123.165301. URL https://link.aps.org/doi/10.1103/PhysRevLett.123.165301.

[44] E. Krotscheck and R. Zillich. Dynamics of He4 droplets. *The Journal of Chemical Physics*, 115(22):10161–10174, 2001. ISSN 0021-9606. doi: 10.1063/1.1400780. URL https://doi.org/10.1063/1.1400780.

[45] J. Peter Toennies. *Helium Nanodroplets: Formation, Physical Properties and Superfluidity*, pages 1–40. Springer International Publishing, Cham, 2022. ISBN 978-3-030-94896-2. doi: 10.1007/978-3-030-94896-2_1. URL https://doi.org/10.1007/978-3-030-94896-2_1.

[46] Sebastian Spicher and Stefan Grimme. Robust Atomistic Modeling of Materials, Organometallic, and Biochemical Systems. *Angewandte Chemie International Edition*, 59(36):15665–15673, 2020. doi: https://doi.org/10.1002/anie.202004239. URL https://onlinelibrary.wiley.com/doi/abs/10.1002/anie.202004239.

[47] H. K. Mao, R. J. Hemley, Y. Wu, A. P. Jephcoat, L. W. Finger, C. S. Zha, and W. A. Bassett. High-Pressure Phase Diagram and Equation of State of Solid Helium from Single-Crystal X-Ray Diffraction to 23.3 GPa. *Phys. Rev. Lett.*, 60:2649–2652, 1988. doi: 10.1103/PhysRevLett.60.2649. URL https://link.aps.org/doi/10.1103/PhysRevLett.60.2649.

[48] Christoph Bannwarth, Sebastian Ehlert, and Stefan Grimme. GFN2-xTB—An Accurate and Broadly Parametrized Self-Consistent Tight-Binding Quantum Chemical Method with Multipole Electrostatics and Density-Dependent Dispersion Contributions. *Journal of Chemical Theory and Computation*, 15(3):1652–1671, 2019. doi: 10.1021/acs.jctc.8b01176. URL https://doi.org/10.1021/acs.jctc.8b01176. PMID: 30741547.

[49] Christoph Bannwarth, Eike Caldeweyher, Sebastian Ehlert, Andreas Hansen, Philipp Pracht, Jakob Seibert, Sebastian Spicher, and Stefan Grimme. Extended tight-binding quantum chemistry methods. *WIREs Computational Molecular Science*, 11(2):e1493, 2021. doi: https://doi.org/10.1002/wcms.1493. URL https://wires.onlinelibrary.wiley.com/doi/abs/10.1002/wcms.1493.

[50] Robert C. Wetzel, Frank A. Baiocchi, Todd R. Hayes, and Robert S. Freund. Absolute cross sections for electron-impact ionization of the rare-gas atoms by the fast-neutral-beam method. *Phys. Rev. A*, 35:559–577, 1987. doi: 10.1103/PhysRevA.35.559. URL https://link.aps.org/doi/10.1103/PhysRevA.35.559.

[51] J.S. Thompson, D.J. Pegg, J. Dellwo, R.N. Compton, and G.D. Alton. Photodetachment of metastable He-. *Nuclear Instruments and Methods in Physics Research Section B: Beam Interactions with Materials and Atoms*, 56-57:211–215, 1991. ISSN 0168-583X. doi: https://doi.org/10.1016/0168-583X(91)96008-9. URL https://www.sciencedirect.com/science/article/pii/0168583X91960089.